Attenuation Field Estimation Using Radio Tomography in Different System Models

M. S. M. Abdullah[1,2], M. H. F. Rahiman[1,2,*], N. S. Khalid[1,3] and A. S. A. Nasir[1,4]

[1] Faculty of Electrical Engineering Technology, Universiti Malaysia Perlis, Pauh Putra Campus, 02600 Arau, Perlis, Malaysia.
[2] Centre of Excellence for Advanced Sensor Technology (CEASTech), Universiti Malaysia Perlis, Pauh Putra Campus, 02600 Arau, Perlis, Malaysia.
[3] Centre of Excellence for Intelligent Robotics & Autonomous Systems (CIRAS), Universiti Malaysia Perlis, Pauh Putra Campus, 02600 Arau, Perlis, Malaysia
[4] Sports Engineering Research Centre (SERC), Universiti Malaysia Perlis, Pauh Putra Campus, 02600 Arau, Perlis.

Corresponding author* email: hafiz@unimap.edu.my
Available online 30 December 2023

ABSTRACT

This study presents a difference between the circle and square model of the RTI system in the monitoring area for localization. the formation of human localization and its uses, detection, monitoring, and quality determination, as the concerns of this research are to detect human and employ an efficient method to monitor and quantify the many objects in a zone by using different systems models which are the circle and square model. Tomographic imaging techniques have been selected as meeting the requirement to be harmless, non-invasive, non-destructive, and capable of visualizing the object inside the monitoring area. A comparison among the frequencies is done for the different algorithms and it is found that the Gaussian algorithm has the highest value overall for both the circle and square system model. MSSIM shows that the difference in the reading the highest of the circle model was 0.791 using the Gaussian algorithm and the highest of the square model was 0.81 using the Gaussian algorithm.

Keywords: Tomography, detection, monitoring

1. Tomography overview

Tomography is a word derived from the Greek, where ‘tomos’ means to slice and ‘graph’ means an image; in other words, tomography can be defined as taking slices of an image. Tomography is the imaging technique, a tomogram is the term for the cross-sectional image of the investigated object, whilst the equipment used to produce the tomogram is called a tomographic system [1]. Process tomography has widely evolved and also been successfully applied in medical applications and industrial applications since the 1970s. This is because it can be applied non-invasively to an object or process of interest in order to extract and interpret important information such as cross-sectional phase compositions, velocity, components concentration measurement, flow rate, and others. Thus, process tomography has attracted the attention of researchers worldwide to investigate and work towards improvements. A digital signal processor-based system is applied for data acquisition and processing as in [2]. The process tomography system is made up of four fundamental parts: a sensor array, an electrical measurement system, a data collection system, and an image reconstruction system.

1.1 Optical Tomography

Optical tomography is the process of the optical illumination of a biological object and calculation of the degree of radiation reflection as a function of the scanned medium’s layer depth [3]. The main feature of OT is the ability to study objects and mediums when the depth of optical radiation propagation is several millimeters and a significant part of the radiation is diffusely scattered and absorbed [4]. One use of the optical tomography technique, known as supernova remnant tomography, is focused on characterizing the various layers of supernova ejecta—the material that the explosion shot outward—through optical spectroscopy[5]. In optical tomography, an item is illuminated with infrared laser beams, and their passage through and scattering by the object are tracked. Researchers attempt to recreate the internal data from observations of the object's border [6].

1.2 Ultrasonic Tomography

This is a system and technique for doing three-dimensional ultrasonic imaging in both transmission mode and reflection mode. [6]. In non-destructive assessment, similar imaging technologies are applicable to a range of different medical issues as well as a variety of non-medical problems.[7] suggested that multimode imaging capacity might be utilized to improve detection of cancer tumors in the human breast [7]. Acoustic tomography includes ultrasonic tomography. It uses ultrasound, whose frequency varies depending on the item being examined; the human body uses ultrasound at a frequency of roughly 2 MHz. The same procedure as in X-ray CT may be used if the object is tiny or nearly homogenous, supposing that the ultrasound propagates rectilinearly. 'The filtered back-projection approach' is the currently most used CT algorithm. [6]. Researchers employed transmission mode for detecting liquid/gas two-phase flow, which is a very inhomogeneous medium, in non-invasive ultrasonic tomography for imaging liquid and gas flow [8].

1.3 Electrical impedance tomography

The method of injecting current into a system or item and monitoring the voltage in order to reconstruct the cross-sectional picture of the body is known as electrical impedance tomography (EIT) [9]. One of the most important techniques for seeing an object's electrical conductivity distribution is EIT, whose hardware. The electrodes are often used as connections to measure voltages. The distribution of conductivity around the item is then determined from the measurement of voltage that will be collected from the receiving electrodes, and is utilized to build and implement a tomographic picture by solving a regularized inverse model. This imaging system technology has an advantage over conventional imaging techniques like PET, CT, and MRI, among others, in that it is at last non-invasive and non-destructive. In the industrial setting, this method is being used [10]. EIT is superior to other imaging techniques in more ways than one, including its comparatively cheap cost compared to other tomographic methods, compactness owing to the lack of a big transducer, simplicity of integration of a purely electronic system, and safety compared to X-ray approaches. [11]. This method's inability to be employed for pneumatic conveyance of big electrically non-conducting solids is one of its key drawbacks. In order to calculate the internal conductivity distribution referring to boundary data, boundary voltage measurements are used to calculate the impedance[12]. This is because the impedance cannot be directly measured [13]. By using dissimilar current injection patterns and sequences of voltage measurement, there are several methods and different strategies to achieve this goal of voltage measurement and each method has its pros and cons.

1.4 Electrical resistance tomography

The electrical resistivity or conductivity of a domain is rebuilt using the border voltage measurement in the imaging technique known as electrical resistance tomography (ERT). [14]. Electrical currents are applied to the boundary of a domain through pairs of electrodes, and their resultant voltages are collected across another pair of electrodes. In a certain experiment, voltages are used as the source and the output currents are measured. The advancement of computer and sensor technologies has gone hand in hand with this. Electrical tomography has a mode called electrical resistance tomography. It has several great qualities, such as being non-invasive, portable, affordable, and having a quick reaction time. In conclusion, the ERT system is mostly used in the detection of concrete structures, measurement of multiphase flow, and medicine.[15], and other aspects.

2. Tomography sensors for Human Application

There are various sensors suggested for use in human tomography. However, the most often used sensors in human research are computed tomography, microwave tomography, and radio tomography. The next section covered tomography sensors, which are frequently employed in human applications, as well as some associated research projects.

2.1 Radio tomography

The RF sensing principle has led to the establishment of the RTI approach, which eventually evolved as one of the most efficient localisation techniques. Across the monitoring wireless sensor network (WSN), this RTI system practically works by exploiting the attenuation of RF signals caused by the presence of targeted objects. It is understood that when the stationary RF sensor nodes are arrayed across the RTI monitoring area, the fluctuation of the RF signals remains unchanged in the absence of a physical object [16]. Consequently, when the targeted object is present within the area, the obstructed transmission links between the associated RF sensor nodes, in terms of received signal strength (RSS) quality, can be assessed to image the location of the targeted object [17]. RSS-based measurement has been extensively used in WSN monitoring and localisation systems because it does not involve the installation of new hardware for a system

development that is already equipped with the RF sensor nodes[18]. The original concept of RSS measurements for the RTI imaging system was proposed by [17]. They utilised the unique transmission links projected between each RF sensor node surrounding the network area. The presence of attenuating object that crosses the unique links will reduce the RSS signal quality in various ways, including absorption, reflection, diffraction and scattering effects on the associated links [19]. Hence, the RTI system computes these RSS shadowing losses to reconstruct the cross-sectional image inside the network area. While RF sensor node deployment is generally simple and affordable, a bigger and more flexible sensing area can be established compared to other approaches which may be infeasible. Besides, unlike infrared imaging systems, RF signals can penetrate through non-metallic boundaries and other obstructions such as trees, furniture and smoke. RF-based imaging by RTI also can perform well even in a dark environment compared to camera-based systems that depend on daylight for better operation[20]. In addition, the RTI system can monitor and localise the targeted subject in real-time without identifying the subject's activities. Therefore, this approach does not evoke a risk of privacy issues.

A. Model of Tomographic Imaging

N sensor nodes are scattered across the monitoring region. Any two sensor nodes may construct a LOS route, and the total number of linkages is indicated as $M = N(N-1)/2$. There are N voxels in the monitoring region. The RSS value changes as a target enters the monitoring region.[21], [17].

$$y = Wx + n \quad (1)$$

Where x is the signal fading value, y is the changes in all of the network's connections, W is the shadow weight matrix, and n is the noise. Some linkages will be blocked when an item is in the imaging region, which will result in significant signal attenuation. Typically, the range is 4-20 dB. Assume Ki is the RSS of link i while there is an object in the region, and $K^e i$ is the RSS when the area is empty. The difference between them, y_i is the shadowing loss of the link i induced by the occlusion of the object.

$$y_i = Ki - K^e i \quad (2)$$

where dBm is the unit. The imaging area is split into several identically sized square parts, each of which is referred to as a pixel, in order to capture a picture of the attenuation that occurs as the signal passes through the area. Assume that there are N total pixels. x_j is the attenuation when the signal passes through the pixel j. Then y_i can be seen as the weighted sum of x_j [17], [22], as represented by the formula

$$y_i = \sum_{j=1}^{N} w_{ij} x_j + n_i \quad (3)$$

In this case, the noise n_i is the result of a signal transmission disturbance, such moisture content. Pixel j weight for link i is w_{ij}. Because attenuation only affects pixels in the LOS path, the weight of pixels that are not in the LOS path should be 0. . Figure 1 shows a wireless network connection that is a LOS route.

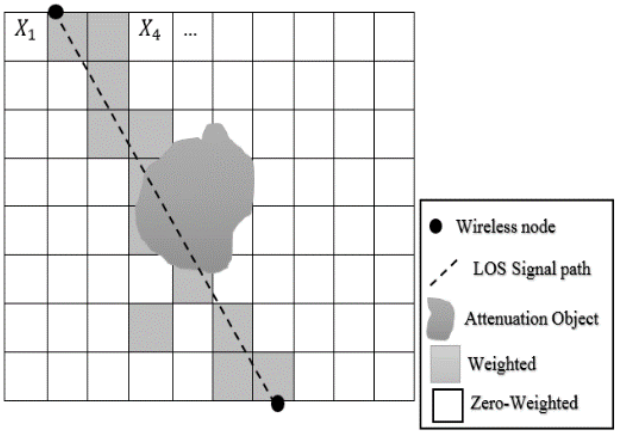

Figure 1 A wireless network connection in a LOS direction

In matrix form, (4) may be expressed as follows to make it seem more condensed.

$$\begin{aligned} y &= WX + n \\ X &= [x_1, x_2 x_3, \ldots . x_N]^T \\ y &= [y_1, y_2, y_3, \ldots . y_M]^T \\ n &= [n_1, n_2, n_3, \ldots . n_M]^T \\ W &= \left[w_{ij}\right]_{M \times N} \end{aligned} \quad (4)$$

Where x is the pixel vector, y is the shadowing loss vector, w is the weight matrix, and n is the noise vector. The weight for each connection in the network is then determined using an elliptical model that we provide [23], [24]. The transmitting and receiving nodes for a certain connection are situated at the ellipse's center. The matching weight is 1 when the pixel is within the ellipse; otherwise, it is 0. Given that there may be variations in the distance between two nodes, the weight will be normalized by the square root of the distance:

$$w_{ij} = \frac{1}{\sqrt{d_i}} \begin{cases} 1 \; if \; d_{ij}(1) + \; d_{ij}(2) < d_i + \delta \\ 0 \; otherwise \end{cases} \quad (5)$$

Where δ is the tunable parameter, which we call the ellipse parameter, describing the width of the ellipse, d_i is the distance between the two nodes, d_{ij} (1) and d_{ij} (2) are the distances between the centre of pixel j and the two nodes respectively for link i.

B. Data Collection Techniques

When a transmitter's signal is applied to an antenna, electromagnetic (EM) waves are transmitted into space. The EM field qualities vary as one moves away from the antenna. As shown in Figure 2, they may be divided into three categories: near field, reactive near field, and far field.

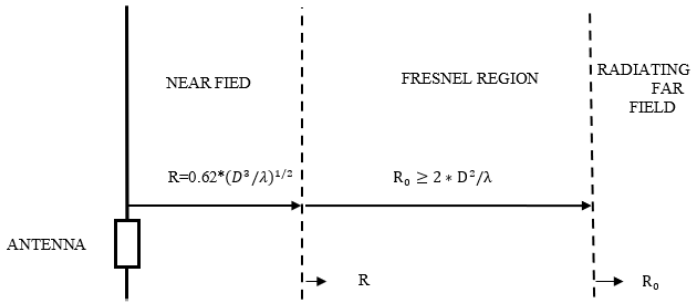

Figure 2 Near and Far Field Regions of an Anttenna.

Equation (6) defines the near field region as the area immediately around the antenna.

$$Near \; field \; Region < \frac{2D^2}{\lambda} \quad (6)$$

where D is the antenna's maximum linear size and is the wavelength of electromagnetic waves.

$$\lambda = \frac{Speed \; of \; Light}{Frequency}$$

No measurements are often conducted there since the fields are mostly unpredictable. Reactive near field refers to the area around the antenna. Electric fields, also known as the E-field, and magnetic fields, sometimes known as H-fields, combine to form electromagnetic waves. Because of their 90-degree phase difference, the E-field and H-field are reactive, as shown by Equation (7). The E/H fields must be orthogonal (perpendicular) and in phase with one another in order to radiate or propagate.

$$Reactive\ Near\ Field\ Region < 0.62\sqrt{\frac{D^3}{\lambda}} \quad (7)$$

Radiative near field: The Fresnel region is another name for this area. This region is located between the reactive near field and the far field. According to Equation (8), the EM fields begin to change from reactive to radiating fields at this point. However, the radiation pattern's form still changes with distance since they haven't fully changed.

$$0.62\sqrt{\frac{D^3}{\lambda}} < Radiative\ Near\ Field\ Region < \frac{2D^2}{\lambda} \quad (8)$$

The far field area follows the radiative near field. The vast bulk of the electromagnetic fields in this region are radiating fields. The E and H fields, like plane waves, are orthogonal to one another and to the direction of propagation. Equation (9) represents the distant field area.

$$Far\ Field\ Region > \frac{2D^2}{\lambda} \quad (9)$$

Antennas are frequently employed in the far-field business to broadcast signals across large distances. To perform measurements in the far-field zone, the distance from the antenna must be significantly greater than the antenna's size and wavelength.

3. System Model

Think on the diagrams in Figure 3 square shape is cover all the area monitoring but circle shape there is gap in some area of the area monitoring. The black dots on the map indicate the positions of the sensors, while the blue lines connecting them show the line-of-sight radio connections between the nodes. The ESP8266 standard was employed by the author of this paper's radio sensors. The benefit of using the algebraic RTI approach, as previously mentioned, was that it allowed for flexibility in the network geometry employed. Basically, any network architecture may be used as long as the positions of the sensors are known.

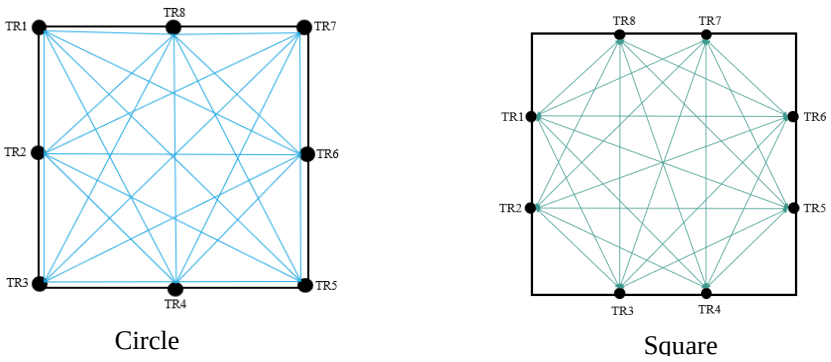

Circle Square

Figure 3 Model of full projection of circle and square model

A. *Sensitivity Maps*

Essentially, the sensitivity function of an array tells us how much a little change in the subsurface resistivity of a specific location will impact the potential measured by that array. With an increase in the sensitivity function's value, the subsurface area has a greater effect on the measurement[25]. A separate array responds to the same sub-surface characteristic in a different way. Some arrays respond more quickly to vertical alterations than others do to horizontal adjustments. Different arrays vary in terms of sensitivity, scope of study, and signal strength. For the normalized sensitivity maps in the case of air as the reference material, an excitation at port j=2, and measurements at ports i= 6 and 8 are shown in Figure 4.

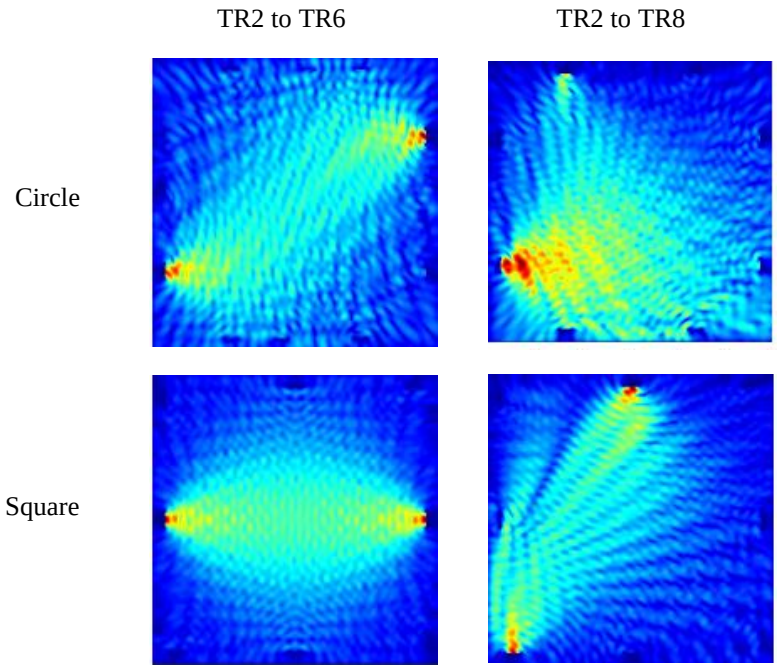

Figure 4 Normalized sensitivity maps of an excitation at RF nodes

4. Results and discussion

The foundation of the radio tomography system that aids in seeing the interior distribution are tomography reconstruction methods. Regularization in MATLAB was employed for the RTI reconstruction. The system used image reconstruction methods that were. In order to draw conclusions about the performance of the suggested radio tomography system, the LBP, FBP, and Gaussian algorithm as well as the image quality of the reconstructed pictures were assessed using the MSSIM image quality evaluation. The circle and square system model used phantom (human) have been designed, as shown in Figure 3, to test and evaluate the proposed system for the different algorithms. Each algorithm has its own features and mathematical properties. In this research, the various proposed phantom has been tested to reconstruct the tomography imaging as shown in figure 6.

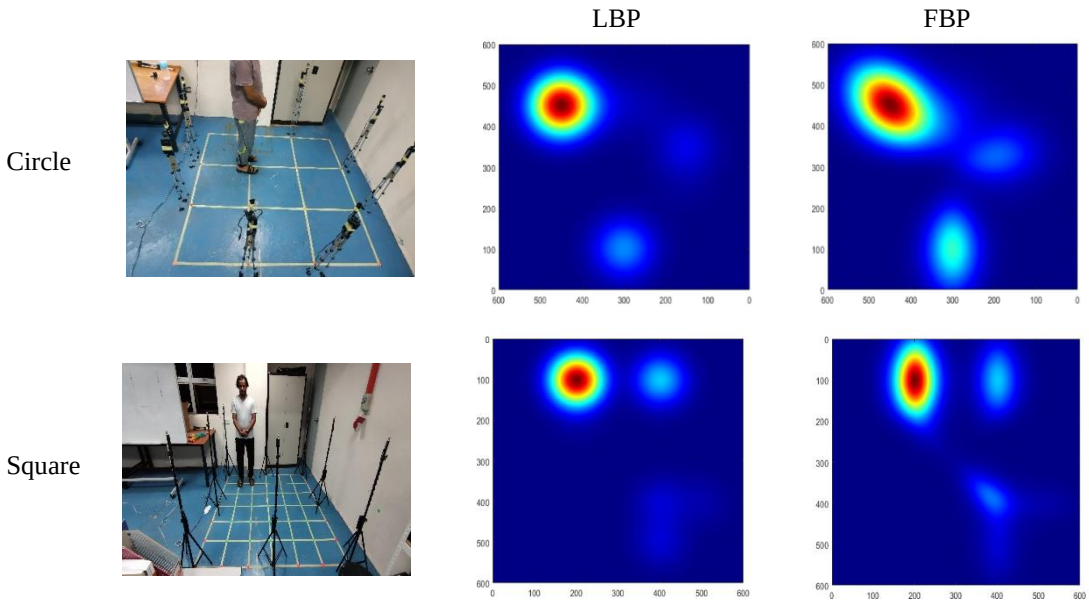

Figure 5 Image reconstruction experiment results in 2D of circle and square system model

The Mean Structural Similarity Index (MSSIM) evaluation test is a useful method for determining the quality of images. Figure 6 shows the experiment phantom in the locations. In this experiment two reconstruction algorithms were involved.

As shown in below the phantom was in a background of air, which was used as the reference. A comparison among the frequencies is done for the different algorithms and it is found that the Gaussian algorithm has the highest value overall for both the circle and square system model. MSSIM shows that the difference in the reading the highest of the circle model was 0.791 using the Gaussian algorithm and the highest of the square model was 0.81 using the Gaussian algorithm.

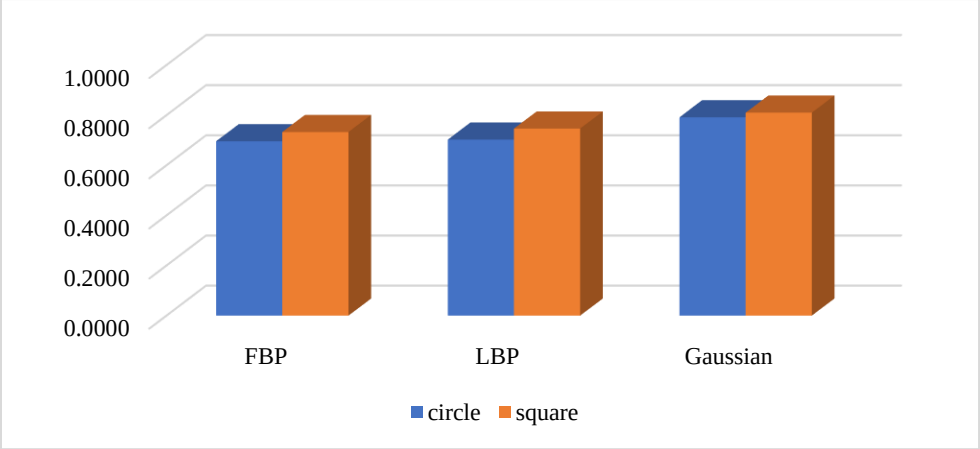

Figure 6 MSSIM indexes computed on reconstructed images of circle and square experiments.

5. Conclusion

This work presents a difference between the circle and square model of the RTI system in the monitoring area for localization. Comparisons made between circle and square RTI system, prove that square model performance is better. Gaussian algorithm and the highest of the square model were 0.81 using the Gaussian algorithm. Square shape RTI system covered all the area monitoring, but circle shape had gap in the area monitoring.

References

[1] M. S. Beck and R. A. Williams, “Process tomography : a European innovation and its applications,” vol. 7, pp. 215–224, 1996.

[2] M. H. F. Rahiman, “Ultrasonic Tomography System For Liquid / Gas Bubble Column,” 2013.

[3] J. Raymond, “Optical Tomography for Supernovae,” *Physics (College. Park. Md).*, vol. 12, Jul. 2019, doi: 10.1103/Physics.12.82.

[4] O. Kalnaya and Y. Kurskoy, “Femtosecond Optical Tomography,” *Metrol. instruments*, no. six issues a year, uniformly in year, pp. 57–60, May 2020, doi: 10.33955/2307-2180(2)2020.57-60.

[5] I. R. Seitenzahl, P. Ghavamian, J. M. Laming, and F. P. A. Vogt, “Optical Tomography of Chemical Elements Synthesized in Type Ia Supernovae,” *Phys. Rev. Lett.*, vol. 123, no. 4, p. 41101, 2019, doi: 10.1103/PhysRevLett.123.041101.

[6] T. Takiguchi, “Ultrasonic tomographic technique and its applications,” *Appl. Sci.*, vol. 9, no. 5, 2019, doi: 10.3390/app9051005.

[7] W. S. Haddad, “SYSTEMAND METHOD FOR ULTRASONIC,” vol. 2, no. 12, 2002.

[8] M. Hafiz, F. Rahiman, R. A. Rahim, M. Hezri, F. Rahiman, and M. Tajjudin, “Ultrasonic Transmission-Mode Tomography Imaging for Liquid / Gas Two-Phase Flow,” vol. 6, no. 6, pp. 1706–1715, 2006.

[9] F. Delbary and R. Kress, “Electrical impedance tomography using a point electrode inverse scheme for complete electrode data,” *Inverse Probl. Imaging*, vol. 2, May 2011, doi: 10.3934/ipi.2011.5.355.

[10] A. Adler, R. Gaburro, and W. Lionheart, “Electrical Impedance Tomography BT - Handbook of Mathematical Methods in Imaging,” O. Scherzer, Ed. New York, NY: Springer New York, 2015, pp. 701–762. doi: 10.1007/978-1-4939-0790-8_14.

[11] T. J. Heindel, J. N. Gray, and T. C. Jensen, "An X-ray system for visualizing fluid flows," *Flow Meas. Instrum.*, vol. 19, no. 2, pp. 67–78, 2008, doi: 10.1016/j.flowmeasinst.2007.09.003.

[12] M. S. M. Abdullah, M. H. F. Rahiman, A. Zakaria, L. M. Kamarudin, and L. Mohamed, "A Review on Moisture Measurement Technique in Agricultural Silos A Review on Moisture Measurement Technique in Agricultural Silos," *IOP Conf. Ser. Mater. Sci. Eng.*, vol. 705, 2019, doi: 10.1088/1757-899X/705/1/012001.

[13] J. Seo and E. J. Woo, "Multi-Frequency Electrical Impedance Tomography and Magnetic Resonance Electrical Impedance Tomography," in *Lecture Notes in Mathematics*, vol. 1983, 2009, pp. 1–71. doi: 10.1007/978-3-642-03444-2_1.

[14] C. Su, J. Zhao, H. Ren, L. Qin, and K. Tian, *Application of Electrical Resistance Tomography*. 2015. doi: 10.2991/icitmi-15.2015.72.

[15] M. Hasan, Y. Shang, H. Meng, P. Shao, and X. Yi, "Application of electrical resistivity tomography (ERT) for rock mass quality evaluation," *Sci. Rep.*, vol. 11, no. 1, pp. 1–19, 2021, doi: 10.1038/s41598-021-03217-8.

[16] S. Shukri, L. Munirah Kamarudin, and M. Hafiz Fazalul Rahiman, "Device-Free Localization for Human Activity Monitoring," *Intell. Video Surveill.*, no. September, 2019, doi: 10.5772/intechopen.79442.

[17] J. Wilson and N. Patwari, "Radio tomographic imaging with wireless networks," *IEEE Trans. Mob. Comput.*, vol. 9, no. 5, pp. 621–632, 2010, doi: 10.1109/TMC.2009.174.

[18] N. A. M. Ramli *et al.*, "A Design and Development of a Wireless Sensor Network for Potential Monitoring and Localization," *J. Electr. Eng. Technol.*, no. 0123456789, 2020, doi: 10.1007/s42835-020-00515-5.

[19] R. Priyadarshini and R. M. Mehra, "Quantitative Review of Occupancy Detection Technologies," no. January, 2015.

[20] M. T. . Talib, M. H. . Rahiman, R. A. Rahim, and M. S. M. Abdulla, "Performance Evaluation of Modified-Hybrid Radio Tomographic Imaging for Human Localization in Outdoor Environment Performance Evaluation of Modified-Hybrid Radio Tomographic Imaging for Human Localization in Outdoor Environment," *J. Tomogr. Syst. Sensors Appl.*, no. September, 2021.

[21] C. Zhu, J. Wang, and Y. Chen, "One New Adaptive Elliptical Weighting Model Combining with Tracking Estimates," *Sensors (Basel)*, vol. 11, no. 9, 2019, doi: 10.3390/s19051034.

[22] H. Liu, Z. H. Wang, X. Y. Bu, and J. P. An, "Image reconstruction algorithms for radio tomographic imaging," *Proc. - 2012 IEEE Int. Conf. Cyber Technol. Autom. Control. Intell. Syst. CYBER 2012*, no. 1, pp. 48–53, 2012, doi: 10.1109/CYBER.2012.6392525.

[23] L. Heng, W. Zheng-huan, B. Xiang-yuan, and A. Jian-ping, "Image Reconstruction Algorithms for Radio Tomographic Imaging," *2012 IEEE Int. Conf. Cyber Technol. Autom. Control. Intell. Syst.*, no. 1, pp. 48–53, 2012, doi: 10.1109/CYBER.2012.6392525.

[24] P. Agrawal and N. Patwari, "Correlated link shadow fading in multi-hop wireless networks," *IEEE Trans. Wirel. Commun.*, vol. 8, no. 8, pp. 4024–4036, 2009, doi: 10.1109/TWC.2009.071293.

[25] M. S. M. Abdullah, M. H. F. Rahiman, N. S. Khalid, and A. S. A. Nasir, "Simulation of Radio Tomographic Imaging for Measurement Rice Moisture Content," *2020 10th IEEE Int. Conf. Control Syst. Comput. Eng. (ICCSCE), Penang, Malaysia, 2020*, pp. 62–67, 2020, doi: 10.1109/ICCSCE50387.2020.9204958.